Asian Journal of Chemistry; Vol. 38, No. 5 (2026), 1153-1158
ASIAN JOURNAL OF CHEMISTRY
https://doi.org/10.14233/ajchem.2026.35526

Synthesis and Characterisation of CuO-Ag Nanocomposites with Enhanced Antimicrobial Activity

P. RAJ SHEKHAR PHANEENDRA[1,2], K. RAGHU[1] and P.V.S. MACHIRAJU[3,*]

[1]Department of Physics, Annamalai University, Chidambaram-608002, India
[2]Department of Physics, Pragati Engineering College (A), Surampalem-533437, India
[3]Faculty of Science, R&D Cell, Malla Reddy (MR), Deemed to be University, Hyderabad-500100, India

*Corresponding author: E-mail: drpvsm.res@gmail.com

Received: 27 December 2025 *Accepted*: 10 March 2026 *Published online*: 4 May 2026 AJC-22339

Metal oxide-metal nanocomposites offer enhanced thermal stability, catalytic efficiency, charge transport, and antimicrobial activity, with performance strongly governed by composition ratio, dispersion, and interfacial quality. The present study reports the synthesis, physico-chemical characterisation and bioactivity of CuO-Ag nanocomposites prepared in three composition ratios (1:2, 1:1 and 2:1), designated as G_1, G_2, and G_3, respectively, *via* a hydrothermal route. The obtained nanocomposites were systematically analysed using FTIR, XRD, SEM, TEM, SAED, XPS, and TGA to evaluate their structural, morphological, compositional and thermal characteristics. FTIR analysis confirmed the presence of Cu–O bonding and interfacial Ag–O–Cu interactions, accompanied by composition-dependent band shifts. XRD patterns revealed the coexistence of monoclinic CuO and face-centred cubic Ag phases. SEM and TEM micrographs showed CuO nanostructures decorated with well-dispersed Ag nanoparticles, indicating effective heterostructure formation. XPS spectra verified the presence of Cu^{2+} species together with metallic Ag. Thermal analysis demonstrated that all samples were stable up to approximately 330 ºC, with G_2 exhibiting the highest thermal resistance. The antimicrobial performance was strongly influenced by composition; G_1 (1:2) displayed the highest antibacterial activity against *Staphylococcus aureus* and notable antifungal efficacy against *Aspergillus niger*, whereas G_3 showed comparatively weak biological activity.

Keywords: Metal, Metal oxide, Composites, Antibacterial, Antifungal.

INTRODUCTION

Among metal oxides, CuO is especially recognised for its strong antimicrobial behaviour, exhibiting broad spectrum activity against various bacterial and viral pathogens [1,2]. CuO nanoparticles have attracted considerable interest owing to their nanoscale dimensions, high surface area, chemical stability and cost-effectiveness, which support their use in diverse technological and biomedical applications [3]. These properties have led to their exploration in wound dressings, topical formulations, coated textiles, disinfection systems and related healthcare applications [4]. They have also shown effective action against clinically relevant microorganisms such as *Escherichia coli*, *Bacillus subtilis* and *Staphylococcus* species [5,6].

The incorporation of silver into metal oxide systems has been widely reported to further enhance catalytic and biological performance. This improvement is generally associated with reduced particle size, accelerated nucleation and growth processes, increased surface reactivity and stronger interactions with microbial cell components or catalytic species. In particular, CuO-Ag hybrid nanostructures exhibit synergistic effects that surpass the performance of the individual constituents [7]. Previous studies have demonstrated that CuO-Ag composites possess distinct physico-chemical properties and significant potential in multiple application areas including antimicrobial coatings, catalysis, sensing and environmental remediation [8]. Moreover, silver and copper-based nanomaterials are considered promising candidates for combating bacterial and viral infections, especially in the context of rising antimicrobial resistance [9,10].

Hybrid CuO-Ag systems have shown improved antibacterial efficacy compared with single-component metal or semiconductor nanoparticles, although their performance strongly depends on factors such as composition ratio, particle size, morphology, surface characteristics and the target microorganism [11]. The hydrothermal method is highly suitable for CuO-Ag nanocomposites, as it enables controlled CuO nanostruc-

ture growth, uniform Ag nanoparticle dispersion and strong interfacial integration, leading to enhanced functional performance [12]. These features are particularly important for tailoring surface dependent properties relevant to biomedical catalytic and applications. Therefore, systematic investigation of composition-dependent CuO-Ag nanocomposites is essential for optimising their structural features and biological activity.

EXPERIMENTAL

All chemicals were of analytical reagent (AR) grade *viz.* including copper sulphate pentahydrate ($CuSO_4·5H_2O$), sodium hydroxide, sodium borohydride ($NaBH_4$), silver nitrate, ethanol and distilled water. Equipment used for synthesis included a Teflon-coated stainless-steel beaker, autoclave and oven to ensure controlled reaction conditions.

Hydrothermal synthesis of CuO-Ag nanocomposite: CuO-Ag nanocomposites were synthesised in three different ratios (1:2, 1:1, 2:1) *via* the hydrothermal method. A 30 mL solution of 0.25 M $CuSO_4·5H_2O$ was mixed with 30 mL of 1 M NaOH to precipitate $Cu(OH)_2$ and Na_2SO_4, stirred for 1 h for homogeneity. A small amount of $NaBH_4$ was added as a reducing agent and then the mixture was divided into three portions and 25 mL of 0.25 M $AgNO_3$ was added dropwise in different ratios to form composites G_1 (1:2), G_2 (1:1) and G_3 (2:1). The solutions were transferred to Teflon-lined autoclaves, heated at 200 ºC for 18 h, cooled to room temperature, washed with ethanol and distilled water, filtered and dried at 60 ºC for 12 h. The resulting green and powdered crystalline CuO-Ag nanocomposites were collected for characterisation.

Characterisation: The FTIR spectra were recorded on a Bruker Alpha spectrometer in the 4000-400 cm^{-1} range using the KBr pellet method with a Techno Search Instruments hydraulic press (Model M15) to confirm composite formation and functional groups. XRD analysis was carried out using a Bruker AXS D8 Advance diffractometer with Cu*K*α radiation over a 2θ range of 20-70º to determine phase composition and crystallinity. Surface morphology was examined by FESEM using a Quanta FEG 450 instrument, while particle size was estimated from micrographs using ImageJ software. The internal morphology and microstructural features were investigated by TEM using a JEOL JEM-2010 microscope operated at 120 kV. Surface elemental composition and oxidation states were analysed using an XPS PHI 5000 VersaProbe III system. Thermal stability was evaluated by thermogravimetric analysis using a Waters (TA Division) Q50 instrument under air atmosphere from 20 to 600 ºC at a heating rate of 20 ºC min^{-1} for all three CuO-Ag nanocomposite samples.

Antibacterial activity: Bacterial strains (*Klebsiella* sp., *Staphylococcus aureus*, *E. coli*, *Bacillus* sp.), MHA/MHB media, standard antibiotic discs (penicillin-G, ampicillin-C, cephalothin-C, erythromycin-T), CuO-Ag nanocomposites (G_1, G_2, G_3), DMSO control, 0.5 McFarland inoculum standard, sterile disposables and basic microbiology equipment. The antibacterial activity was assessed using the Kirby-Bauer disc diffusion method following CLSI guidelines [13,14]. The bacterial cultures were adjusted to 0.5 McFarland and spread onto MHA plates. Discs impregnated with G_1, G_2 or G_3 were placed on inoculated plates along with DMSO (negative control). Plates were incubated at 37 ºC for 24 h and the zone of inhibition (ZOI) was measured to determine antibacterial activity.

RESULTS AND DISCUSSION

FTIR studies: The CuO-Ag nanocomposites with different composition ratios, namely G_1 (1:2), G_2 (1:1) and G_3 (2:1), were characterised by FTIR spectroscopy. All samples exhibited broad absorption bands in the 3588-3563 cm^{-1} and 3406-3375 cm^{-1} region, assigned to O–H stretching vibrations of surface hydroxyl groups, along with weak bands near 1630 cm^{-1} corresponding to H–O–H bending of adsorbed moisture [13-15] (Fig. 1). The characteristic metal-oxygen (M–O) vibrations were observed in the lower wavenumber region. The peaks at 1131 cm^{-1} for G_1 and 1117-1160 cm^{-1} for G_3 were attributed to Cu–O and interfacial Ag–O–Cu stretching modes, while peaks within 779-690 cm^{-1} were associated with Cu–O lattice vibrations. The appearance of peaks in the 917-883 cm^{-1} region was assigned to Ag–O or Cu–O–Ag linkages and at 532-464 cm^{-1} corresponded to the bending vibrations of Cu–O–Cu and Ag–O–Cu bonds [16]. The progressive shifts and intensity variations observed from G_1 to G_3 suggest the composition-dependent structural modification, enhanced metal–oxygen interactions and increased heterogeneity with changing CuO/ Ag ratio, while G_2 exhibited the most balanced interfacial interaction between CuO and Ag phases. The absence of significant organic-related bands indicates effective precursor decomposition and the formation of high-purity CuO-Ag nanocomposites suitable for applications [17].

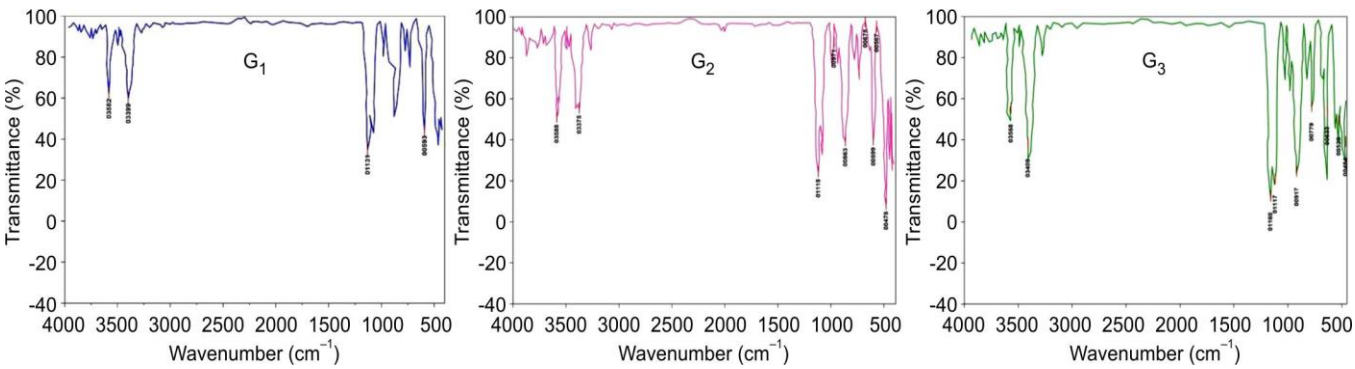

Fig. 1. FT-IR spectra of CuO-Ag nanocomposite G_1 (1:2), G_2 (1:1) and G_3 (2:1)

XRD studies: The crystalline structure and phase composition of the CuO-Ag nanocomposites (G_1, G_2 and G_3) were examined by X-ray diffraction using Cu*K*α radiation (λ = 1.54059 Å) over a 2θ range of 5-90º (Fig. 2). The diffraction patterns confirmed the coexistence of monoclinic CuO and face-centered cubic (FCC) Ag phases. The characteristic reflections of CuO were observed at 2θ values of 33.32º, 35.48º and 52.4º, consistent with JCPDS card no. 48-1548, while peaks at 39.6º and 44.3º correspond to the (111) and (200) planes of metallic Ag (JCPDS card no. 04-0783).

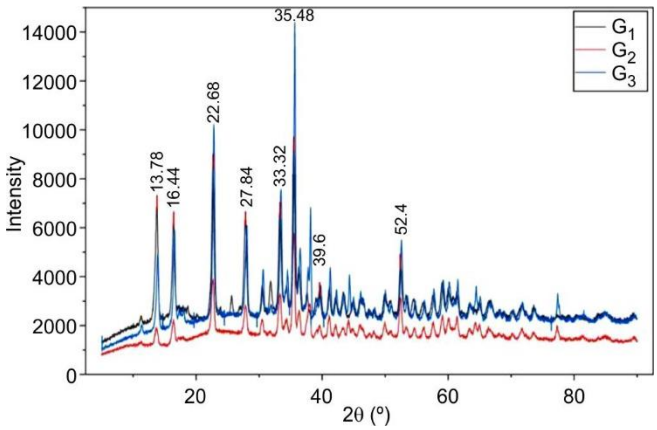

Fig. 2. XRD spectrum of CuO-Ag nanocomposites

Sample G_1 exhibited well-resolved CuO peaks with moderate intensity, indicating good crystallinity. In contrast, G_2 sample showed broader and less intense reflections, suggesting reduced crystallite size, lattice distortion or strain arising from Ag incorporation into the composite structure. Sample G_3 displayed sharp and intense diffraction peaks for both CuO and Ag phases, confirming effective in situ reduction of Ag^+ ions and improved crystallinity of the nanocomposite [18,19]. The progressive enhancement of Ag reflections with increasing Ag content demonstrates successful phase formation and strong interfacial interaction between CuO and Ag.

SEM studies: The SEM analysis of the CuO-Ag nanocomposites G_1 (1:2), G_2 (1:1) and G_3 (2:1) showed that the Ag/CuO ratio strongly affects surface morphology and particle distribution (Fig. 3). Composite G_1 exhibited densely packed and irregular agglomerated clusters, which may be attributed to rapid nucleation and growth induced by higher Ag content [20]. In contrast, G_2 displayed well-defined flower-like hierarchical nanostructures with moderate agglomeration, indicating favourable interfacial interaction and balanced growth between CuO and Ag phases [21]. Sample G_3, containing higher CuO content, showed more uniform plate-like nanostructures with comparatively lower aggregation [22]. Particle size analysis of G_2 further revealed nanosheets decorated with Ag nanoparticles having an average size of approximately 73 nm, confirming the nanoscale nature of the composite. These results suggest that the equimolar CuO-Ag ratio in G_2 yields the utmost homogeneous and structurally optimised morphology, making it a suitable candidate for detailed TEM investigation.

TEM studies: TEM analysis of the G_2 (1:1 CuO-Ag) nanocomposite revealed well-defined rectangular to cuboidal CuO nanocrystals uniformly decorated with Ag nanoparticles (Fig. 4a-d). The CuO particles exhibited sharp edges and flat facets, indicating high crystallinity and anisotropic growth, while Ag nanoparticles were distributed over the surfaces, edges and facet junctions, suggesting strong interfacial interaction between the two phases. The SAED patterns shown in Fig. 4e-f displayed distinct rings and diffraction spots indexed to monoclinic CuO and face-centered cubic Ag, confirming the crystalline nature and coexistence of both components. Thus, the TEM and SAED results verify the successful formation of a crystalline CuO-Ag heterostructure with extensive interfacial contact.

XPS studies: The XPS spectrum of the CuO-Ag (1:1) nanocomposite confirmed the presence of Cu and Ag on the surface (Fig. 5). The Cu 2p spectrum showed the characteristic Cu^{2+} doublet of monoclinic CuO, while the Ag 3*d* peaks at 368.3 eV ($3d_{5/2}$) and 377.0 eV ($3d_{3/2}$) correspond to metallic Ag nanoparticles [23]. No significant chemical shifts or satellite features were observed, indicating the coexistence of CuO and metallic Ag. The results are correlated well with the TEM and SAED observations, confirming the successful formation of a CuO-Ag heterostructure.

Thermal studies: Thermogravimetric analysis (TGA) of CuO-Ag nanocomposites (G_1, G_2, G_3) showed all samples are stable up to ~330 ºC, with initial weight losses of 0.32-0.41% due to adsorbed moisture (Fig. 6). Major decomposition occurs between 330-590 ºC, corresponding to the breakdown of organic residues and precursor-derived components, with weight losses of 12.9-13.6%. Sample G_2 exhibited the highest

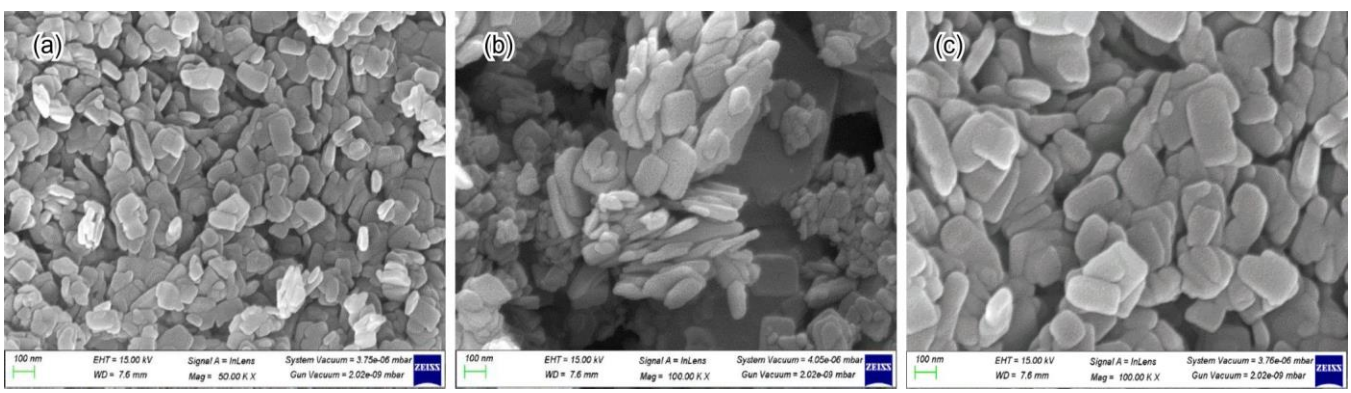

Fig. 3. SEM images of CuO-Ag nanocomposites synthesised in CuO:Ag ratios [(a) G_1 (1:2), (b) (G_2 (1:1) and (c) G_3 (2:1)]

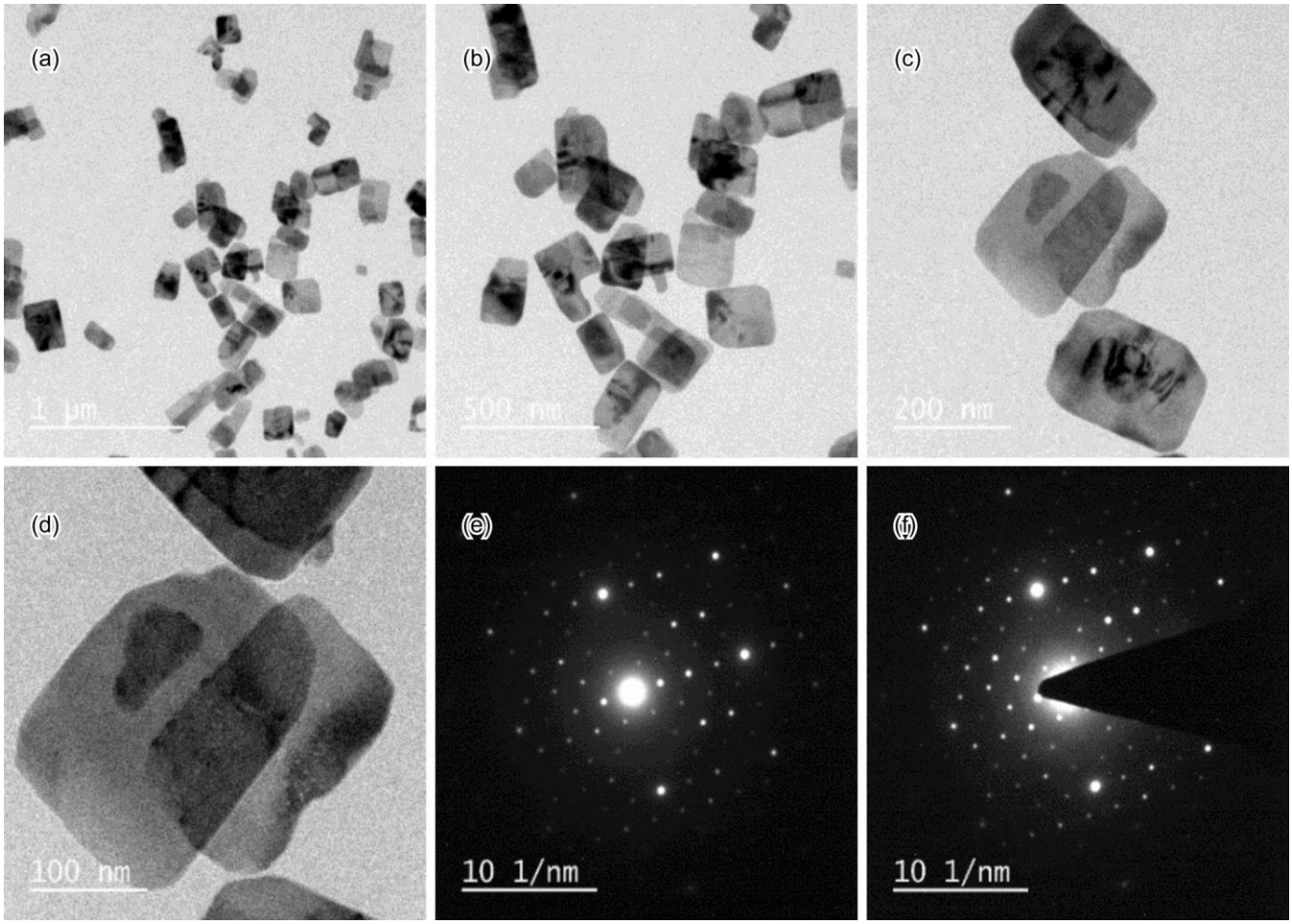

Fig. 4. TEM images of CuO-Ag nanocomposites and SAED patterns

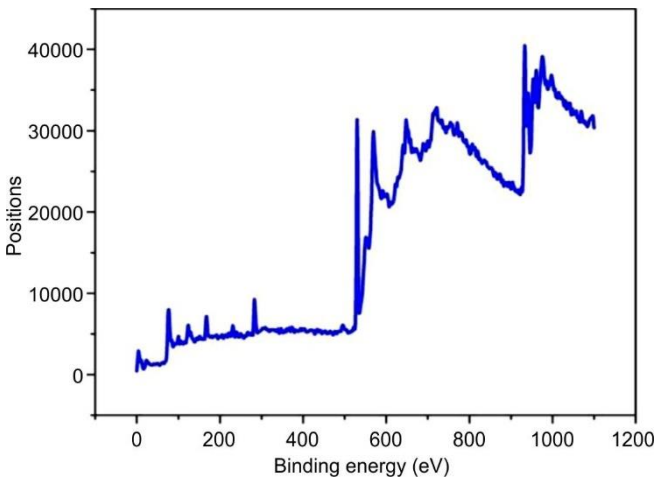

Fig. 5. XPS spectra of CuO-Ag nanocomposite

thermal stability, retaining ~87.1% residual mass, while sample G_3 shows the lowest stability due to higher organic content and moisture. In all, G_1 demonstrates the intermediate behaviour. The thermal stability follows the order $G_2 > G_1 > G_3$, confirming that a balanced CuO-Ag ratio enhances nanocomposite stability.

Antibacterial activity: The antibacterial activity of CuO-Ag nanocomposites was evaluated by the zone of inhibition (ZOI) method against *Klebsiella* sp., *Staphylococcus aureus*, *Escherichia coli* and *Bacillus* sp., using DMSO as negative control. The control showed no inhibition, confirming that the observed antibacterial effects were solely due to the nanocomposites. The enhanced activity of CuO-Ag systems is attributed to the synergistic action of CuO and Ag nanoparticles, which can generate reactive oxygen species (ROS), release Cu^{2+} and Ag^{+} ions, disrupt bacterial membranes, denature proteins and damage nucleic acids, ultimately leading to cell death [24-29]. The electrostatic interaction between released metal ions and negatively charged bacterial cell surfaces further promotes membrane destabilisation and intracellular damage [30-34]. Previous studies have also shown that Ag/CuO nanocomposites exhibit superior antibacterial performance compared with individual CuO or Ag nanoparticles due to combined metallic-semiconductor effects [35-40].

Among the tested samples, G_1 exhibited the highest antibacterial activity, producing a 14 mm inhibition zone against *S. aureus*, 9 mm against *Klebsiella* sp. and 4 mm against *Bacillus* sp., while no detectable inhibition was observed against *E. coli*. Samples G_2 and G_3 showed only negligible or weak inhibition against most strains and were similarly inactive against *E. coli* (Table-1). Thus, sample G_1 demonstrated moderate activity against *S. aureus* and weak activity against the remaining susceptible strains. The relative anti-

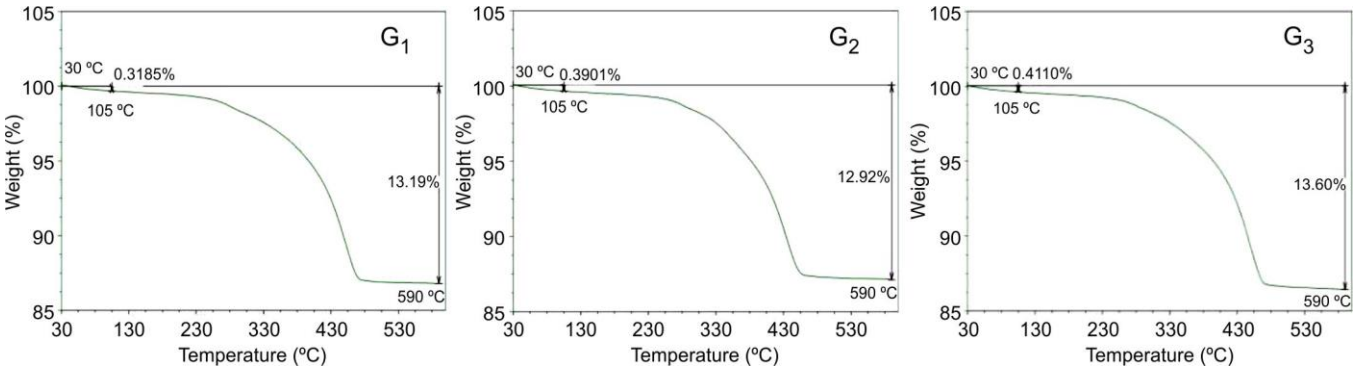

Fig. 6. Thermograms of (a) G_1, (b) G_2 and (c) G_3 samples

TABLE-1
ZONE OF INHIBITION (mm) OF G_1-G_3 SAMPLES AGAINST SELECTED BACTERIAL STRAINS

Specimen/bacterial species	*Klebsiella* sp. (mm)	*S. aureus* (mm)	*E. coli* (mm)	*Bacillus* sp. (mm)
Control (DMSO)	0	0	0	0
G_1 (1:2)	9	14	0	4
G_2 (1:1)	0	4	0	4
G_3 (2:1)	4	0	0	4

bacterial order was $G_1 > G_3 > G_2$ for *Klebsiella*, $G_1 > G_2 > G_3$ for *Staphylococcus aureus* and $G_1 = G_3 > G_2$ for *Bacillus* sp. while all nanocomposites remained ineffective against *E. coli*. Based on these results, it is concluded that the CuO-Ag nanocomposites were more effective against Gram-positive bacteria than Gram-negative bacteria, likely due to the absence of the protective outer membrane in Gram-positive cell walls. The antibacterial behaviour was strongly dependent on the CuO/Ag composition ratio, with G_1 (1:2) emerging as the most promising material.

Antifungal activity: The antifungal activity against *A. niger* showed a strong dependence on the CuO-Ag composition ratio. Among the tested samples, G_1 (1:2) exhibited the highest antifungal efficacy, producing a distinct zone of inhibition corresponding to 28% growth suppression, indicating effective inhibition of fungal proliferation. Sample G_2 (1:1) demonstrated moderate activity, with a measurable inhibition zone and 20% growth inhibition. In contrast, sample G_3 (2:1) showed no detectable zone of inhibition and 0% antifungal activity, suggesting that higher CuO content is less effective under the studied conditions. The DMSO control produced no inhibitory response, confirming that the observed antifungal activity originated solely from the CuO-Ag nanocomposites. These results indicate that antifungal performance is strongly governed by the CuO-Ag ratio, with the Ag-rich G_1 (1:2) nanocomposite emerging as the most effective formulation against *A. niger*.

Conclusion

The CuO-Ag nanocomposites with different composition were successfully synthesised by a hydrothermal method and investigated for their structural, thermal and antimicrobial properties. FTIR, XRD, SEM, TEM, SAED and XPS analyses confirmed the formation of crystalline CuO-Ag heterostructures consisting of monoclinic CuO and metallic Ag with effective interfacial contact. The CuO/Ag ratio significantly influenced morphology, crystallinity and thermal behaviour. Among the prepared samples, G_2 (1:1) showed the most uniform morphology and highest thermal stability indicating that a balanced composition favours structural integrity. Antimicrobial studies revealed strong composition-dependent activity. The G_1 (1:2) nanocomposite exhibited the highest antibacterial performance, particularly against *S. aureus* and also showed the best antifungal activity against *A. niger*. In contrast, the G_3 (2:1) sample displayed weak biological activity. The improved performance of G_1 is attributed to the synergistic effect of CuO and Ag, which promotes the reactive oxygen species generation, metal ion release and microbial membrane disruption. Thus, the results demonstrate that the compositional tuning is an effective strategy to optimise CuO-Ag nanocomposites for the multifunctional applications.

ACKNOWLEDGEMENTS

The authors express their gratitude to the Department of Physics, Annamalai University and R&D Cell, Pragati Engineering College for their support.

CONFLICT OF INTEREST

The authors declare that there is no conflict of interests regarding the publication of this article.

DECLARATION OF AI-ASSISTED TECHNOLOGIES

During the preparation of this manuscript, the authors used an AI-assisted tool(s) to improve the language. The authors reviewed and edited the content and take full responsibility for the published work.

REFERENCES

1. S. Chanthee, J. Jirasangthong, C. Asasvatesanupap and M. Santikunaporn, *Mater. Miner.*, **32**, 68 (2022); https://doi.org/10.55713/jmmm.v32i3.1270

2. R.B. Asamoah, E. Annan, B. Mensah, P. Nbelayim, V. Apalangya, B. Onwona-Agyeman and A. Yaya, *Adv. Mater. Sci. Eng.*, **2020**, 7814324 (2020); https://doi.org/10.1155/2020/7814324
3. S. Naz, A. Gul, M. Zia and R. Javed, *Appl. Microbiol. Biotechnol.*, **107**, 1039 (2023); https://doi.org/10.1007/s00253-023-12364-z
4. M.E. Grigore, E.R. Biscu, A.M. Holban, M.C. Gestal and A.M. Grumezescu, *Pharmaceuticals*, **9**, 75 (2016); https://doi.org/10.3390/ph9040075
5. S. Baker, P. Olga, R. Tatiana, P. Nadezhda, G. Tatyana, R. Tatyana, E. Saveleva, K. Olga, G. Elizaveta, G. Karina, U. Ekaterina, S. Anastasia and P. Margarita, *J. Genet. Eng. Biotechnol.*, **18**, 53 (2020); https://doi.org/10.1186/s43141-020-00068-0
6. S. Naz, A. Gul, M. Zia and R. Javed, *Appl. Microbiol. Biotechnol.*, **107**, 1039 (2023); https://doi.org/10.1007/s00253-023-12364-z
7. S. Arya, Prerna, A. Singh and R. Kour, *Mater. Res. Express*, **6**, 116313 (2019); https://doi.org/10.1088/2053-1591/ab49ab
8. M.B. Gawande, A. Goswami, F.X. Felpin, T. Asefa, X. Huang, R. Silva, X. Zou, R. Zboril and R.S. Varma, *Chem. Rev.*, **116**, 3722 (2016); https://doi.org/10.1021/acs.chemrev.5b00482
9. G.R. Tortella, J.C. Pieretti, M. Fernández-Baldo, A. Benavides-Mendoza, O. Rubilar, M.C. Diez and A.B. Seabra, *Crit. Rev. Biotechnol.*, **42**, 431 (2022); https://doi.org/10.1080/07388551.2021.1939260
10. A. Norouzi, S. Mansouri, R. Mardani, M.H. Nematollahi, M. Abolhassani, M. E. Norouzmahani, A. Najmadini, A.A. Sardari and G. Asadikaram, *ChemistrySelect*, **9**, e202304776 (2024); https://doi.org/10.1002/slct.202304776
11. N. Ghasemi, F. Jamali-Sheini and R. Zekavati, *Mater. Lett.*, **196**, 78 (2017); https://doi.org/10.1016/j.matlet.2017.02.111
12. H.H. Almutairi, N. Parveen and S.A. Ansari, *Nanomaterials*, **12**, 4167 (2022); https://doi.org/10.3390/nano12234167
13. A.W. Bauer, W.M.M. Kirby, J.C. Sherris and M. Turck, *Am. J. Clin. Pathol.*, **45**, 493 (1966).
14. I. Gajic, J. Kabic, D. Kekic, M. Jovicevic, M. Milenkovic, D. Mitic Culafic, A. Trudic, L. Ranin and N. Opavski, *Antibiotics*, **11**, 427 (2022); https://doi.org/10.3390/antibiotics11040427
15. B.V. Krishna, B.D. Lakshmi, P.T. Rao and R.K. Ramachandra, *Results Mater.*, **26**, 100695 (2025); https://doi.org/10.1016/j.rinma.2025.100695
16. M. Rashad, M. Rüsing, G. Berth, K. Lischka and A. Pawlis, *J. Nanomater.*, **2013**, 714853 (2013); https://doi.org/10.1155/2013/714853
17. D. Manyasree, K.M. Peddi and R. Ravikumar, *Int. J. Appl. Pharm.*, **9**, 71 (2017); https://doi.org/10.22159/ijap.2017v9i6.71757
18. L.G. Devi and R. Kavitha, *Appl. Catal. B Environ.*, **140-141**, 559 (2013); https://doi.org/10.1016/j.apcatb.2013.04.035
19. A.T. Mosleh, E.A. Kamoun, S.H. EL-Moslamy, S.A. Salim, H.Y. Zahran, S.H. Zyoud and I.S. Yahia, *Discover Nano*, **19**, 166 (2024); https://doi.org/10.1186/s11671-024-04108-3
20. C. Parvathiraja and S. Shailajha, *Appl. Nanosci.*, **11**, 1411 (2021); https://doi.org/10.1007/s13204-021-01743-5
21. M.J. Javid-Naderi, Z. Sabouri, A. Jalili, H. Zarrinfar, S. Sammak and M. Darroudi, *Environ. Technol. Innov.*, **38**, 104147 (2025); https://doi.org/10.1016/j.eti.2025.104147
22. M. Farooq, S. Shujah, K. Tahir, S.T. Hussain, A.U. Khan, Z.M. Almarhoon, K.F. Alabbosh, A.A. Alanazi, T.M. Althagafi and M.E.A. Zaki, *Sci. Rep.*, **14**, 1618 (2024); https://doi.org/10.1038/s41598-024-51391-2
23. J. Huang, F. Tang, C. Gu, C. Shi and M. Zhai, *Front. Optoelectron.*, **5**, 429 (2012); https://doi.org/10.1007/s12200-012-0293-7
24. H. Li, Y. Zou and J. Jiang, *Dalton Trans.*, **49**, 9274 (2020); https://doi.org/10.1039/D0DT01816C
25. B. Uma, K.S. Anantharaju, B.S. Surendra, K. Gurushantha, S.S. More, S. Meena, B. Hemavathi and H.C.A. Murthy, *ACS Omega*, **8**, 9947 (2023); https://doi.org/10.1021/acsomega.2c07124
26. G. Vasiliev, A.-L. Kubo, H. Vija, A. Kahru, D. Bondar, Y. Karpichev and O. Bondarenko. *Sci. Rep.*, **13**, 9202 (2023); https://doi.org/10.1038/s41598-023-36460-2
27. C.Y. Leong, R.A. Wahab, S.L. Lee, V.K. Ponnusamy and Y.-H. Chen, *Environ. Res.*, **227**, 115578 (2023); https://doi.org/10.1016/j.envres.2023.115578
28. J. Chen, S. Mao, Z. Xu and W. Ding, *RSC Adv.*, **9**, 3788 (2019); https://doi.org/10.1039/C8RA09186B
29. S.M.A.A. Mousavi, S.A. Mirhosseini, M.R.S. Panahi and H.M. Hosseini, *Probiotics Antimicrob. Proteins*, **12**, 740 (2020); https://doi.org/10.1007/s12602-019-09530-z
30. M.-L. Kung, M.-H. Tai, P.-Y. Lin, D.-C. Wu, W.-J. Wu, B.-W. Yeh, H.-S. Hung, C.-H. Kuo, Y.-W. Chen, S.-L. Hsieh and S. Hsieh, *Colloids Surf. B Biointerfaces*, **155**, 399 (2017); https://doi.org/10.1016/j.colsurfb.2017.04.041
31. H. Saravanan, T. Subramani, S. Rajaramon, H. David, A. Sajeevan, S. Sujith and A.P. Solomon, *Front. Pharmacol.*, **14**, 1282073 (2023); https://doi.org/10.3389/fphar.2023.1282073
32. B. Le Ouay and F. Stellacci, *Nano Today*, **10**, 339 (2015); https://doi.org/10.1016/j.nantod.2015.04.002
33. M.I. Nabila and K. Kannabiran, *Biocatal. Agric. Biotechnol.*, **15**, 56 (2018); https://doi.org/10.1016/j.bcab.2018.05.011
34. S. Jadhav, S. Gaikwad, M. Nimse and A. Rajbhoj, *J. Cluster Sci.*, **22**, 121 (2011); https://doi.org/10.1007/s10876-011-0349-7
35. W.-R. Li, X.-B. Xie, Q.-S. Shi, H.-Y. Zeng, Y.-S. OU-Yang and Y.-B. Chen, *Appl. Microbiol. Biotechnol.*, **85**, 1115 (2010); https://doi.org/10.1007/s00253-009-2159-5
36. S. Meghana, P. Kabra, S. Chakraborty and N. Padmavathy, *RSC Adv.*, **5**, 12293 (2015); https://doi.org/10.1039/C4RA12163E
37. S.M. Dizaj, F. Lotfipour, M. Barzegar-Jalali, M.H. Zarrintan and K. Adibkia, *Mater. Sci. Eng. C*, **44**, 278 (2014); https://doi.org/10.1016/j.msec.2014.08.031
38. O. Bondarenko, K. Juganson, A. Ivask, K. Kasemets, M. Mortimer and A. Kahru, *Arch. Toxicol.*, **87**, 1181 (2013); https://doi.org/10.1007/s00204-013-1079-4
39. S. Huang, D. Ma, Z. Hu, Q. He, J. Zai, D. Chen, H. Sun, Z. Chen, Q. Qiao, M. Wu and X. Qian, *ACS Appl. Mater. Interfaces*, **9**, 27607 (2017); https://doi.org/10.1021/acsami.7b05418
40. S. Singh, K. Barick and D. Bahadur, *Nanomater. Nanotechnol.*, **3**, 20 (2013); https://doi.org/10.5772/57237